TTHE PENNSYLVANIA STATE UNIVERSITY
SCHREYER HONORS COLLEGE

DEPARTMENT OF ENGINEERING SCIENCE AND MECHANICS

EVALUATING THE ULTRASONIC RESPONSE OF SHAPE MEMORY ALLOYS

TREVOR W. GRIM

SPRING 2021

A thesis submitted in partial
fulfillment of the requirements for a
baccalaureate degree in Engineering Science
with honors in Engineering Science

Reviewed and approved* by the following:

Andrea P. Arguelles
Assistant Professor of Engineering Science and Mechanics
Thesis Supervisor

Joseph Cusumano
Professor of Engineering Science and Mechanics
Honors Adviser

Judith A. Todd
Department Head
P.B. Breneman Chair and Professor of Engineering Science and Mechanics

* Electronic approvals on file in the Schreyer Honors College and Engineering Science and Mechanics Office.

ABSTRACT

Lay Abstract:

When most people think of ultrasound, they picture a mother receiving one during pregnancy. However, ultrasound is a beneficial tool in better understanding various materials and their microstructures. Using the same technology as medical ultrasound, researchers can map materials at the micron level without having to break them open. One material group that has yet to be fully explored is shape memory alloys. Shape memory alloys are materials that can be deformed at one temperature and returned to their initial shape after heating. While this sounds surprising at first, shape memory alloys are not all that uncommon, appearing in airplanes, orthodontic braces, and many other areas. A large, broad study of shape memory alloys must be completed in order to fully understand their microstructures. This includes studying alloys of similar compositions manufactured different ways and at several points throughout deformation. Before doing such a study, however, a set procedure must be created with sample experiments laying out benchmarks of how to identify microstructural changes within an ultrasonic map. By improving our understanding of their microstructures with ultrasound, shape memory alloys can be made safer, cheaper and better for applications ranging from eye glasses to space ships.

Technical Abstract:

Through mechanical and thermal stimulation, metallic shape memory alloys (SMAs) can be deformed and undeformed. SMAs are widely used in the medical and aerospace industries due to their versatility and affordability. One way to improve shape memory alloys is to better understand their microstructures which is served well by ultrasonic investigation. To do this, an expansive study must be conducted analyzing SMAs differentiated by manufacturing process and microstructure throughout deformation. Before such an expansive study can be completed,

however, a set procedure must be set for doing so. Through analyzing five different NiTi SMAs of different microstructural phase (martensitic or austenitic) and different manufacturing methods (cast, wrought, or additively manufactured), benchmarks for analyzing SMAs with ultrasound were set and a procedure for further investigation was outlined. While general trends were noticed between wrought and additively manufactured (AM) samples, with wrought samples having higher attenuation and AM samples having higher wave speeds, more measurements will be needed to exactly link ultrasonic phenomena and microstructural features.

TABLE OF CONTENTS

LIST OF FIGURES

LIST OF TABLES

ACKNOWLEDGEMENTS

The completion of this thesis would have been impossible without the unending devotion and expertise of my research advisor, Dr. Andrea P. Arguelles. From Venezuelan politics, to the intricacies of Bracketology, to the depths of ultrasonic physics, speaking to and learning from Dr. Arguelles was one of the privileges of my time at Penn State. I also owe a debt of gratitude to my parents for their unending support and for encouraging me to apply for enough scholarships in high school that it impressed my now employer so that I could spend this year working on my thesis instead of searching for jobs. Finally, I would like to thank my girlfriend and roommate for not letting me take myself too seriously and for providing enough distraction that I made myself schedule concrete times to complete this thesis. At the end of my life, I'd like a eulogy, not a resume, and these people have helped me live a life that I hope to be worthy of one.

INTRODUCTION

Problem Statement

Shape memory alloys (SMAs) have the potential to revolutionize various industries throughout the world. Their unique ability to change shape without mechanical stimulation leads to their versatility and interest. Before they can be implemented more broadly, however, it is beneficial to better understand their microstructures. One of the best ways to do this is to analyze a large quantity of SMAs differentiated by their manufacturing processes, microstructural phase, and alloy composition along with testing them throughout their deformation such as at different points throughout a tensile test. In doing this, microstructural characteristics can be attributed to specific qualities of different SMAs. Ultrasonic characterization serves as a useful tool to provide accurate microstructural maps. Ultrasound provides accurate and consistent measurements unencumbered by the destruction of samples. Because ultrasound is nondestructive, it lends itself to in situ analysis of samples which is especially pertinent with SMAs. An investigation into how such a large quantity of tests can be completed efficiently and accurately is needed. Such an analysis could take years to complete and an abundance of funding. A set procedure can streamline this process and lead to better results overall. By testing several different SMAs with ultrasound, an accurate procedure for future testing can be created with benchmarks for how to identify and pair different microstructural phenomena with their explanations.

Design Needs

The experimental procedure is iterative yet customizable dependent on the sample shape and material as outlined below in the methodology. The scope of the investigation is not in the experiments themselves, but in the potential impact the research can have on a global scale.

Because SMAs are used so much in the medical industry, understanding them better can lead to better public health overall. Better public health disproportionately affects those in poorer communities globally. Creating cheaper and better SMAs in medical applications provides better safety for the world's poorest and rapidly improves their way of life. Stronger and more versatile SMAs also lead to safer aerospace technologies which can protect pilots and astronauts during flight. Finally, because ultrasonic testing is nondestructive, it is more sustainable than other examination procedures. Cultural, social and environmental factors were also considered, though this research's effect on them are less profound.

LITERATURE REVIEW

Shape memory alloys (SMAs) are materials that can be deformed mechanically and then, through non-mechanical stimulation (either thermal, magnetic or chemical), be returned to their original shape [1]. Metallic SMAs are heavily researched and invested in, particularly those relying on thermal stimulation. Most people have some experience with metallic SMAs. Orthodontic braces must continuously shrink to maintain constant pressure on the teeth in order to straighten them out. Shape memory behavior is directly linked to the metal's microstructure as shown in Figure 1. At a given temperature, depending on the specific material, the metal is in the martensitic phase. Here, the molecules are not packed as tightly or symmetrically which leaves the metal more susceptible to deformation. After mechanical deformation at this low temperature, the metal maintains a martensitic structure. However, when heated, the metal undergoes a phase transformation into austenite which more tightly packs the atoms into a very symmetric shape. Once cooled, the SMA regains its martensitic structure in its original shape [2].

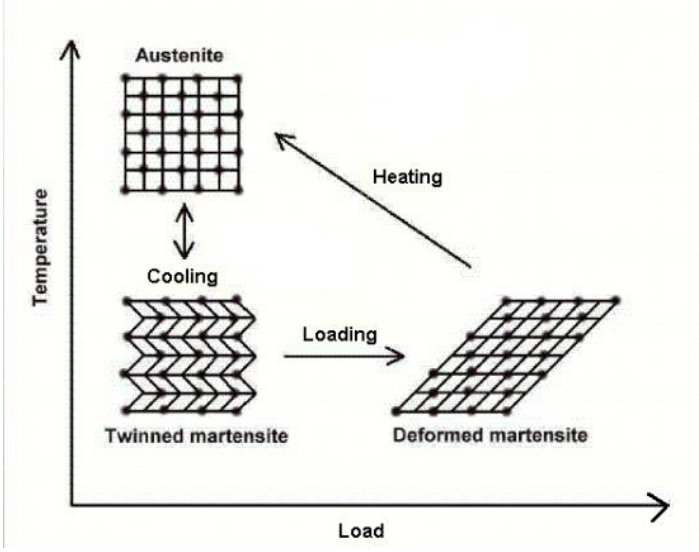

Figure 1: At low temperatures, metals are in the martensitic phase. When a load is applied, the metal deforms. As the metal is heated, the microstructure undergoes a phase change into austenite which, when cooled, returns the metal to its original shape and microstructure [3].

SMAs come in all shapes and sizes and can be made up of many different metals (see Table 1). However, since their inception in 1963, Nickel Titanium (NiTi) alloys have become the most widely used. This is due to their high thermal conductivity, corrosion resistance and formability [4]. These properties also make NiTi SMAs perfect for medical applications, which is where they are most widely used. For example, NiTi SMAs are used in stents where they are crimped down and placed in arteries. Once they are placed, they return to their original shape thus holding the arteries open for unobstructed blood flow. After setting, their extreme flexibility and corrosion resistance allow the stents to hold up to the activity of even the most active of adults [5]. These alloys are also used in bone plates where it is important for pressure to constantly be applied to the fusing bones. SMAs in this case shrink as the bone fuses due to the warm body temperature. In doing so, the SMA keeps constant pressure on the two bones until they fuse [3]. Perhaps the most well-known SMA application is in braces. A similar principle is applied for braces as is for bone plates. The NiTi wire in braces continually contracts, keeping constant pressure on the teeth in order to straighten them.

SMAs are also widely used in the aerospace industry where flexibility and durability are of the utmost importance. In fact, NiTi was first discovered in the Naval Ordnance Laboratory which is why NiTi is commonly known in industry as nitinol. Learning more about SMAs will help create cheaper, better and safer SMAs for the future. Linking their microstructures to performance will aid greatly in this task.

Table 1: Properties of Different Metallic SMAs [6]

Alloys	Composition Atomic or Weight Percent	Transformation Temperature Range (Celsius)
Ag - Cd	44/49 at.%	-190 to -50
Au - Cd	46.5/50 at.%	30 to 100
Cu - Al - Ni	14/14.5 wt% 3/4.5 wt%	-140 to 100
Cu - Sn	approx. 15 at%	-120 to 30
Cu - Zn	38.5/41.5 wt%	-180 to -10
Cu - Zn - (Si,Sn,Al)	a few wt.% of (Si, Sn,Al)	-180 to 200
In - Ti	18/23 at%	60 to 100
Ni - Al	36/38 at%	-180 to 100
Ni - Ti	49/51 at%	-50 to 110
Fe - Pt	approx. 25 at% Pt	approx. -130
Mn - Cu	5/35 at% Cu	-250 to 180

When analyzing SMAs, it is vital to understand the microstructure of the alloy. After all, that is where the magic happens. It is important to focus on highly localized characterization in-situ using non-destructive methods. This, in the end, is more efficient and cost effective because testing the same parts repeatedly cuts down on the cost of excessive parts and allows for the comparison of samples to themselves throughout deformation processes. To this point, one of the best ways to investigate SMAs has been through highly localized characterization using transmission electron microscopes (TEMs). TEMs provide very high resolution images of microstructures at magnifications down to one nanometer [7]. Scientists must remember that changes seen at a microscopic level do not necessarily manifest themselves in the macro world where industrial applications come into play. By looking at images taken at different points throughout a deformation process, researchers can identify exactly what happens when an SMA is subject to thermal or mechanical loads [8]. Therefore, it is beneficial in exploring the microstructural changes undergone between martensite and austenite as the SMA is deformed and then heated up. Figure 2 shows TEM imaging of martensitic stainless steel being deformed,

displaying the power TEMs provide in analyzing in-situ microstructural changes. TEM analysis of microstructures has been done since the invention of the TEM in the early 1930's by Knoll and Ruska, an invention that won Ruska the Nobel Prize in 1986 [9]. TEM microscopy has been useful in investigating "conventional imaging, electron diffraction, chemical microanalysis, high resolution imaging and magnetic structure imaging Lorentz microscopy" [10]. The high spatial resolution provided by TEM analysis allows researchers to look at the actual microstructures of materials in addition to grain boundaries and dislocations.

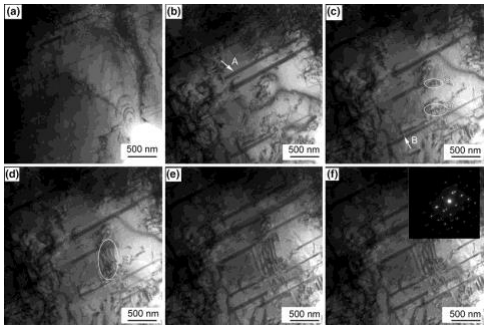

Figure 2: Martensitic stainless steel as it is deformed from 30 μm in frame b up to 80 μm in frame f. It is evident how beneficial TEM imaging is in tracking microstructural changes as the differences between frame a and f are seen through visual analysis [11].

Digital Image Correlation (DIC) is another method researchers use to analyze mechanical behavior. DIC uses highly advanced cameras to track changes in an object overtime [12]. DIC is an extremely sensitive measuring system that can detect deformations, strains, vibrations or changes in contour [13]. DIC has been used in the past to "characterize physical phenomena governing mechanical material behavior" [14]. Researchers used DICs on SMAs to detect heterogeneities within the grain structure in austenite and martensite, but the samples could only be one grain thick. Though DIC is great at measuring small changes in geometric properties, it really cannot compare to the microstructural images that TEM provides. Hence, TEM's usefulness in highly localized characterization of SMAs.

As previously mentioned, when analyzing structures at the microscopic level, it is important to be cognizant of the challenges associated with upscaling to the macro level. Effects that are important on a macro level become negligible at the micro level [15]. Likewise, effects that are subjects of entire areas of study on the micro scale can more or less be ignored when looking at the big picture. For example, on the macro scale, gravity is a force that must always be accounted for. This is not so on the micro scale. At the microscopic level, gravity becomes negligible and surface forces such as friction and surface tension are prominent. Correspondingly, at the macro level, friction and surface tension do not play as key a role. Fortunately, unlike discussions surrounding the nano scale, intrinsic properties of materials themselves generally do not change between the macro and micro scales. Density, texture and the validity of thermodynamics are all generally maintained when transitioning between the macro and the micro [15]. This is beneficial in analyzing SMAs because so much of SMA use is dependent on these intrinsic material properties. At the nano scale, however, classical physics fades away and is overtaken by quantum mechanics which complicates matters much more. Here, the validity of thermodynamics is questioned and it is more difficult to see changes in the nano scale manifested in the macro scale. In sum, effects seen in the material at a microscopic level do not necessarily manifest themselves in practical applications at the macroscopic level because there are different mechanisms that dominate in each sphere. It is important to keep this in mind when investigating SMAs.

Finally, because SMAs have such a broad range of application and the research into their microstructure has only scratched the surface, it is important to investigate them in an accurate and efficient manner. To do this, analysis should be done in-situ, in bulk and non-destructively. In-situ analysis is essential for SMAs where microstructural evolution is the focus of the

research. Tracking how SMAs change when subjected to certain loads or temperatures is necessary in order to understand the material at all. Bulk analysis is necessary because the function SMAs serve in industry is the subject of the research overall. Bulk analysis tracks how smaller, structural changes affect the material's overall function. As previously mentioned, changes in the nano scale do not necessarily manifest themselves the same way in the macro scale. While changes in the micron range shown through TEM analysis are more likely to show themselves at the macro scale, measurements taken on the millimeter range may be more indicative of SMA behavior while in service. SMAs are now and will continue to be used in bulk at the industrial level. Lastly, non-destructive testing (NDT) is beneficial because it is cheap, quick and does not interfere with the function of the actual specimen. Non-destructive testing allows for repeatable tests on a singular sample [16]. This lends itself to in-situ analysis because a sample can be analyzed at different points in a transformation or at different points throughout mechanical deformation. Non-destructive testing is also less expensive than destructive testing. This is rather evident. If a sample can be tested multiple times and then used in the field, it is cheaper than destroying samples after one test and never being able to use a previously tested sample in industry. NDT provides field testing capabilities as well. In the aerospace industry, where SMAs are frequently used, it is difficult (sometimes impossible) and expensive to remove an in-use part for analysis. NDT can examine specimens while they are active to provide structural checks in an efficient manner. Unfortunately, TEMs are not an NDT method because the samples they use are so thin (down to a micron) that they cannot analyze parts in the field, parts that have the potential to be used in industry or macroscopic specimens at different points in a test [17]. The inability of TEMs to be used non-destructively opens the door for other, less known NDT methods in the search to understand different SMA microstructures.

Ultrasound has emerged as a suitable tool to characterize microstructures in materials. Though most people know it as a tool to see babies in the womb, the same technique can be used to detect flaws within materials and map microstructural compositions. Ultrasound meets the criteria mentioned earlier in that it is non-destructive and can be done in-situ and in bulk. In this domain, the change in acoustic wave propagation speed can be measured to see how SMAs change microstructurally when exposed to varying thermal and mechanical stimulations [18]. By tracking the speed changes throughout the specimen, researchers are capable of locating and characterizing changes in interatomic bonds that accompany such stimulation. Ultrasound is also used to calculate elastic constants within the material which "brings valuable information on redistribution of stresses and energy during nucleation of martensite in the austenitic matrix, which is related to substantially different mechanical properties of the phases" [19]. To calculate the elastic constants, all that is needed are the transverse and longitudinal wave propagating velocities, denoted by $V_T$and $V_L$in the equations below. From there, using equations 1, 2 and 3, with ρ being the density, it is relatively simple to calculate Poisson's ratio, μ, the elastic modulus, E and the shear modulus, G [20].

Equation 1: $\mu = \frac{1-2*(V_T/V_L)^2}{2-2*(V_T/V_L)^2}$

Equation 2: $E = \frac{{V_L}^2\rho(1+\mu)(1-2\mu)}{1-\mu}$

Equation 3: $G = {V_T}^2\rho$

Using these equations, researchers can track how the constants change with temperature which is beneficial to understanding most metals. Unfortunately, these equations assume isotropy for the material, an assumption that most SMAs defy. To correct this misplaced

assumption, models would need to be drastically changed, or multiple anisotropic SMA samples would need to be tested [21]. Elastic constants are of course vital to material science because they help show how materials react to stresses and strains. Within SMAs, they can help determine how they deform and their properties throughout the undoing of their deformation. Ultrasound is much better at calculating these constants than traditional mechanical tests because it provides instantaneous data about wave velocities, which when coupled with material densities, allows for extremely accurate and precise measurements of elastic constants. Figure 3 shows just some of the capabilities ultrasound is beginning to provide. Because different phases of metals often have different elastic constants, the wave velocities through those phases will be different. Therefore, by tracking and recording the wave velocities throughout an entire specimen, one can see exactly what phases are present and where.

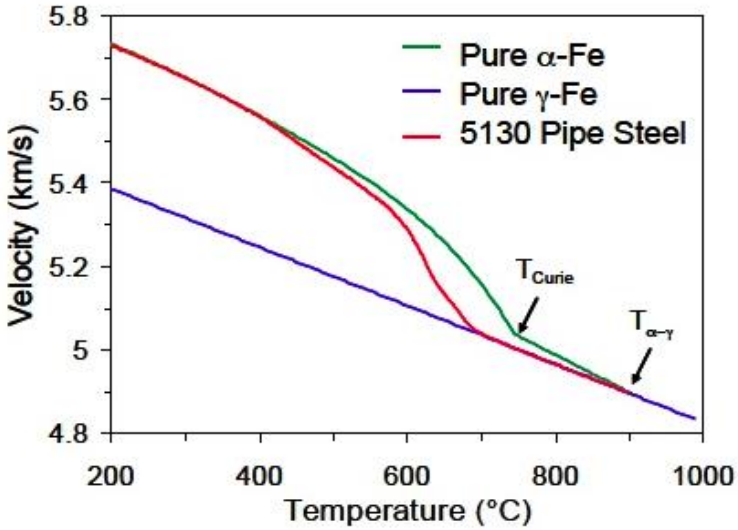

Figure 3: By tracking the wave velocities through 5310 pipe steel as it's heated, one can witness the phase transformation from austenite to ferrite. Here we can see that ferrite's velocity decreases more gradually than that of austenite [22].

Though ultrasound has been used for decades in calculating elastic constants in metals and plastics, it is relatively new to do so in shape memory alloys which is both exciting and daunting [23].

Ultrasound has more capabilities than just detecting flaws and finding elastic constants. Ultrasound can help map microstructures spatially to discover more about their properties. In fact, innovations in ultrasonics have allowed researchers to record hundreds of measurements in a few minutes that have taken days and weeks to record using regular metallurgical studies [22]. Through measuring the attenuation of scattering ultrasonic pulses, it is possible to measure the grain growth and size. A good way to measure grain size is to measure how much attenuation occurs throughout a specimen. Where there is more scattering, the grain size will be bigger. Smaller grain sizes lead to less attenuation.

Using ultrasound to map microstructures is rapidly gaining in popularity and frequency. Though its application began with standard metals such as steel and iron, recently its versatility has been displayed. In 2016, the National Institute of Health published a paper discussing ultrasound's usefulness in tissue engineering [24]. Engineering biological tissue is a monumental scientific achievement; one that has just recently been taken commercial. Therefore, engineers needed a way to non-destructively analyze the tissue while in use. They have begun using ultrasound to analyze the microstructures of engineered and natural tissue to compare them and make sure the engineered tissue behaves properly. Additionally, analyzing the microstructures allows for the certification of healthy rather than diseased tissue. Ultrasound's portability, penetration depth and range of applicable frequencies make it useful in this field, which implies its utility in other arenas.

Another arena ultrasound has made its way into is that of additively manufactured (AM) metals. AM metals have begun to take industry by storm with the aerospace, automobile and robotics industries leading the way [25]. Analyzing the attenuation and backscatter of AM metals allows for analysis of microstructure morphology and the calculation of microhardness and grain

size. As described earlier, larger grain size leads to higher attenuation. Larger grain size also leads to a smaller microhardness [26]. Figure 4 shows results published recently in *Ultrasonics* showing attenuation across wrought, AM and hybrid AM stainless steel samples [27]. It is evident that the wrought and AM samples are mostly uniform, with the AM sample showing attenuation along the edge. This makes sense because they were both manufactured uniformly. The hybrid AM sample exhibits cyclical attenuation due to its manufacturing technique where individual layers were cold worked through laser peening as the sample was being additively manufactured [28]. From looking at the attenuation, it can be seen that the grain size increases from the wrought to the AM to the hybrid AM samples. This means that the hardness decreases in the same direction; a result confirmed from destructive tests recorded in the same study. Because ultrasound provides sensitive and therefore accurate measurements, it is a good tool for characterizing material properties and mapping microstructures. Sotelo showed its applicability with AM samples. A similar process can be completed for SMAs [27].

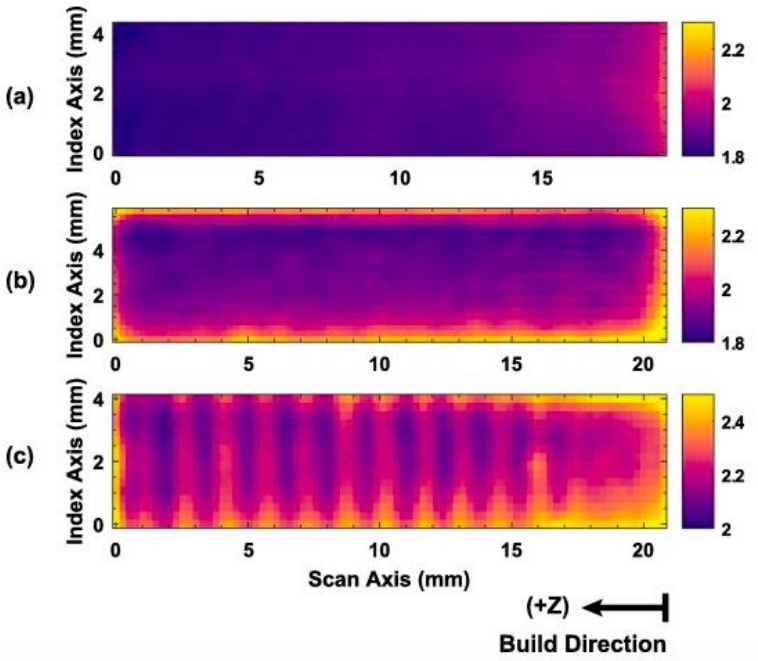

Figure 4: Attenuation of (a) wrought, (b) AM and (c) hybrid AM stainless steel samples from Sotelo [27].

Because SMAs are so versatile and are so prominent in the medical and aerospace industries, it is essential to further explore them and better understand their microstructures. TEM imaging has been useful in the past but takes a lot of time and money to operate and process. It also requires extraordinarily thin samples which renders it near useless in the field. Non-destructive ultrasound provides a less expensive, more versatile alternative that can measure in-situ and in bulk. Though it is more widely known in the medical industry, ultrasound has been instrumental in detecting flaws and calculating material elastic constants for decades. More recently, ultrasound has been applied in tissue engineering and in mapping microstructures of wrought and AM metals. In the search to best understand the microstructures of SMAs as they transform, ultrasound seeks to play the paramount role. Below, a study is described where different SMAs were subject to ultrasonic testing in order to map their microstructures and better understand their properties.

METHODOLOGY

Materials

Five NiTi samples were tested, differentiated by their alloy composition, manufacturing technique, and microstructural phase. The first sample was a polycrystalline NiTiNb cast alloy. The next two samples were polycrystalline NiTi wrought alloys with 50.3 wt.% Ti. Of these two samples, an austenitic sample was 49.2 wt. % Ti and a martensitic sample was 49.7 wt. % Ti. Finally, two AM specimens were tested, both martensitic. Both were Ti rich NiTi alloys produced through the laser directed energy technique with a feedstock composed of 53.1 wt.% Ti and 46.9 wt.% Ni. One of these samples was built in flat tension where the smallest dimension is built in the vertical plane. The other was built in standing tension with the largest dimension built in the vertical plane. The densities for all samples were assumed to be 6500 $^{kg}/_{m^3}$.

Experimental Procedure

In order to characterize the microstructure of the various SMAs, pulse-echo ultrasonics were used in a water immersion tank with a 25 MHz transducer. An immersion tank was used because surrounding a sample with water minimizes the signal interference between the transducer and the sample and provides a uniform couplant. Supports are used to lift the sample off the base of the tank and fully surround the sample with water. Supports are also used to raise the sample closer to the transducer in order to bring it into proper focus. Figure 5 shows the basic setup of the experiments with arrows detailing how the ultrasonic pulses interact with the samples. The front surface reflection is that which is caused by the initial interaction of the signal with the sample. The remaining, unreflected signal then moves through the sample before being reflected back to the transducer by the back wall. This phenomenon continues, with the signal

reflecting off the of the front and back walls, until several back wall reflections are recorded and the ultrasonic signal eventually fades into noise.

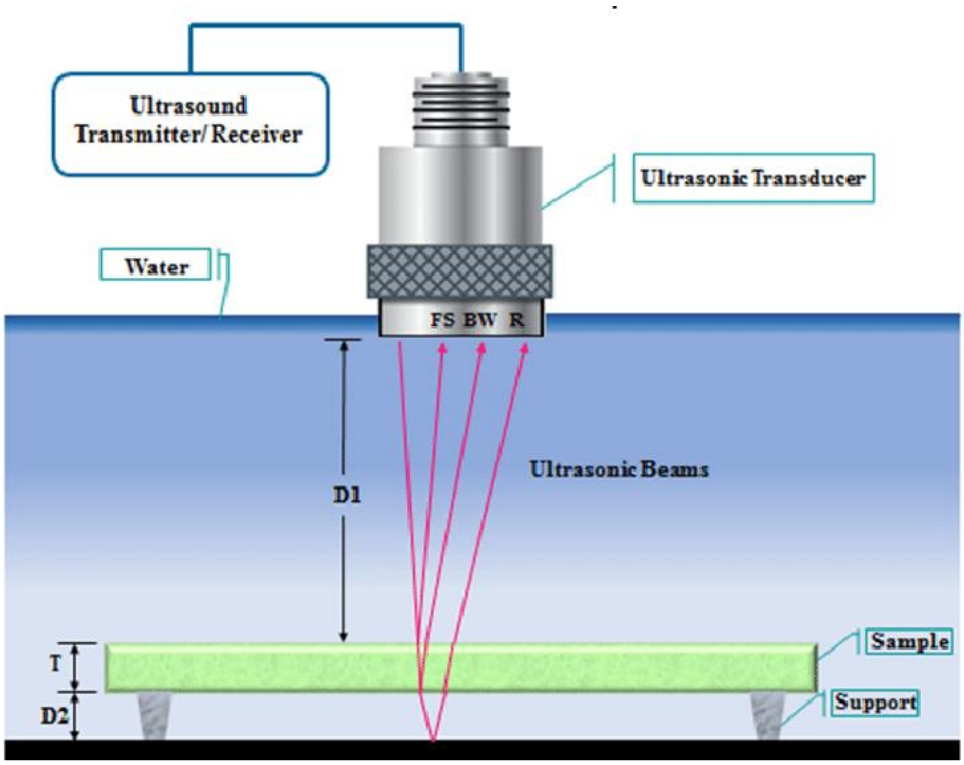

Figure 5: A single transducer both sends and receives ultrasonic beams. FS is the front wall reflection, BW is the first back wall reflection and R is the reflection from the bottom of the tank. R was not recorded in the experiments of this study because the standoffs raised the sample high enough off of the base of the tank that R faded into noise. The figure does not display a focused transducer, which is elaborated upon below and in Figure 6 [29].

A 1" focus allowed for sensitivity and increased resolution throughout the tests. As shown in Figure 6, focused transducers center the pulses at a given location. For the purposes of these experiments, the signal was focused on the back wall of the samples. Before performing the experiments, the samples were measured for length, width and height in order to complete an accurate scan. Dog bone specimens were used because the samples analyzed may be tensile tested and analyzed again in the future. A university supplied computer operating software programs UTWin and JSR was used for all five samples. The experiments were done with the transducer running a 50 MHz low pass filter and a 12.5 MHz high pass filter at 300V and a gain of 5 db. The system ran at 14.8 J with damping and trigger settings of 44 Ω and 50 Ω,

respectively. Each sample was run over a 4 mm x 15 mm area so that the necks of the dog bone specimens were fully captured. The scans were completed at a sampling rate of 1 and a step size of 0.1 mm.

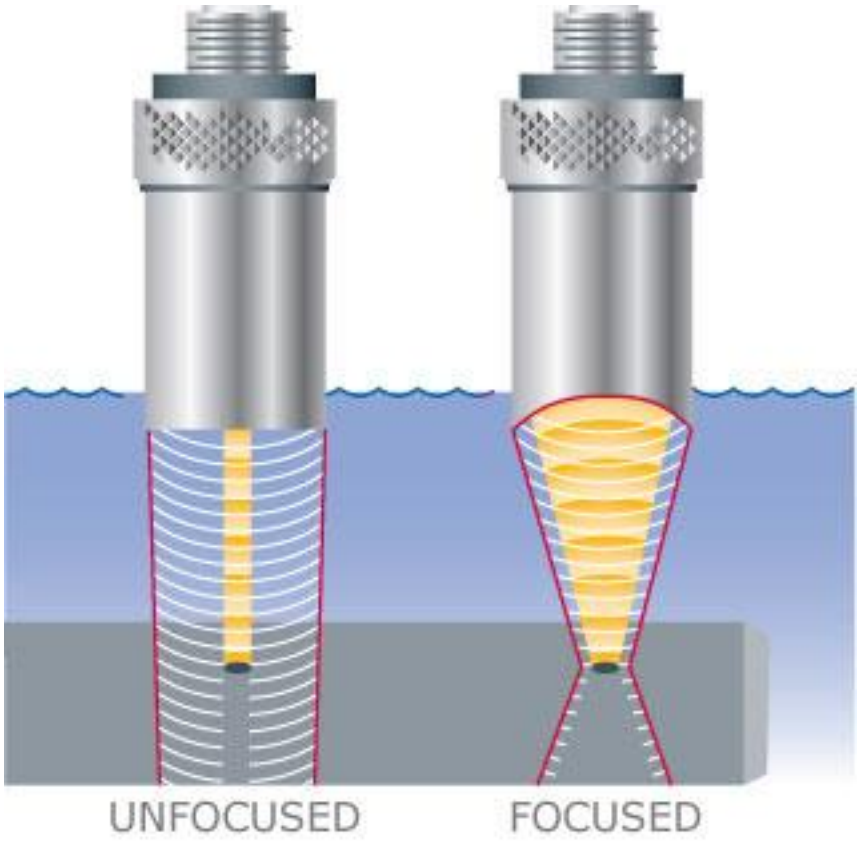

Figure 6: Focused transducers employ a curved surface which allows for the signal to converge at a given distance, 1"in this case. An unfocused transducer has a flat surface that sends a broad, non-converging signal. Focused transducers supply a higher sensitivity and resolution [30].

After setting up the software, the water path was calculated in millimeters and microseconds using equations 4 and 5.

Equation 4: $WP_{mm}=F-MP\frac{C_m}{C_w}$

Equation 5: $WP_{\mu s}=\frac{2WP_{mm}}{C_w}$

Where WP_{mm} and $WP_{\mu s}$ are the water paths in units of mm and s, F is the focal distance in mm, MP is the material path in mm and C_m and C_w are the speed of sound in the material and in the water in units of m/s and are 5924 and 1486, respectively. The material path is the distance in mm into the sample that the signal is focused. The water path is the time in seconds that it takes for an ultrasonic signal to reach the front wall of the sample at a given focal distance and material path. Table 2 shows the samples tested with their respective dimensions and water paths.

Table 2: Dimensions and Water Paths of the Five Samples

Sample	Neck Dimensions (h x w x t) (mm)	Water Path (mm)	Water Path (μs)	Water Path Differential with Silica Sample (mm)
NiTiNb Cast	12.30 x 3.05 x1.016	21.44	28.85	-3.018
NiTi Wrought Martensite	12.57 x 3.03 x 0.95	21.70	29.20	-3.364
NiTi Wrought Austenite	11.61 x 2.98 x 0.95	21.70	29.20	-3.364
AM FT	11.90 x 3.02 x0.97	21.62	29.10	-3.259
AM ST	11.68 x 3.01 x 0.98	21.58	29.04	-3.210

After calculating the water path of the signal, manual and automatic leveling were performed to position the transducer at the correct distance from the sample. Leveling must be done to assure that the transducer remains the correct distance from the sample throughout scanning. Scans were then completed keeping the front wall and first three back wall reflections within view. C-scans were done with the parameters listed above. The last step of the experimental procedure is to complete a scan of a 1.5875 mm thick silica specimen in order to

account for transducer effects throughout testing and normalize system parameters for the absolute calculations of attenuation shown below.

Data Processing

After testing, the .csv files exported from UTWin (the scanning software) were uploaded to and run through a MATLAB code provided by Olivia Cook, found in Appendix A. After adjusting for sample thickness, density and center frequency, and identifying the boundaries of the front wall and first back wall, the code produces attenuation and wave speed maps of the samples. These maps can then be compared with each other to identify their microstructural differences. Wave speed and attenuation are calculated using equations 6 and 7:

$$\text{Equation 6: } v = \frac{2t}{t_d}$$

$$\text{Equation 7: } \alpha_s = \frac{1}{2t} \ln \left\{ \frac{B_r(w) R_s \left(1 - {R_s}^2\right)}{B_s(w) R_r \left(1 - {R_r}^2\right)} e^{2\alpha_f WP_{diff}} \right\} \text{ [27]}$$

Where t is the thickness of the sample, t_d is the time differential between when the transducer sends and receives the signal, $B_r(w)$ and $B_s(w)$ are the amplitudes of the first wall in the silica and the SMA, respectively, R_r and R_s are the silica and SMA reflection coefficients, respectively, α_s is the attenuation of the fluid, and WP_{diff} is the difference in the water paths between the silica sample and the SMA. The cross-correlation method was employed to find the time delay.

RESULTS AND DISCUSSIONS

Due to the presence of Nb in the cast sample, it is unfavorable to compare it with the rest of the samples which are all NiTi alloys. However, it is still beneficial to compare the attenuation and wave speed maps to SEM images taken of the microstructure itself. Figure 7 shows the ultrasonic maps and an SEM image of the cast sample at 500X magnification provided by the Hamilton group. The SEM image showcases the eutectic microstructure of the cast sample with its cellular-like boundaries representing an Nb-phase. The ultrasonic maps match the boundaries shown on the SEM image by also showing a eutectic Nb with a cellular-like boundary morphology [31].

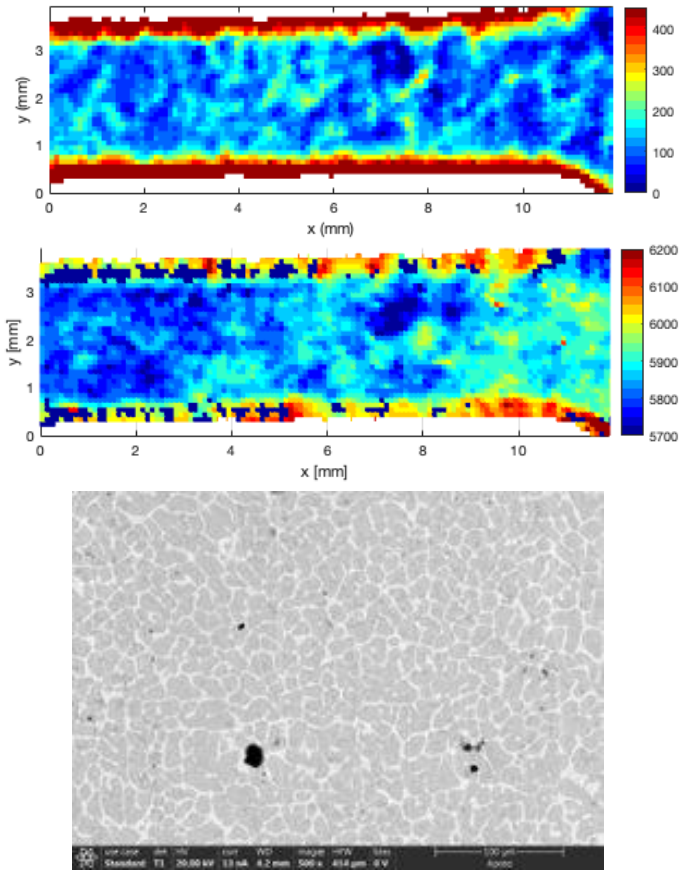

Figure 7: Attenuation (Np/m), Wave Speed (m/s), and SEM maps of the cast sample provided by the Hamilton group. The SEM image is at 500 μm across the bottom. Grain boundaries can be seen in all three, though more information about internal phenomena can be deduced from ultrasound.

The ultrasonic maps also provide insight as to the length-scale of the grain boundaries which are much finer than the eutectic. Different grain sizes and orientations affect how the ultrasonic pulses propagate through the material, which is how the maps identify and portray the boundaries. The cast sample had the highest average wave speed of all of the five samples but had a comparable average attenuation. It is difficult to attribute this wave speed to anything specific so, in the future, it would be beneficial to obtain a cast NiTi sample without Nb so it can be more directly compared to the other samples and more insightful conclusions can be drawn.

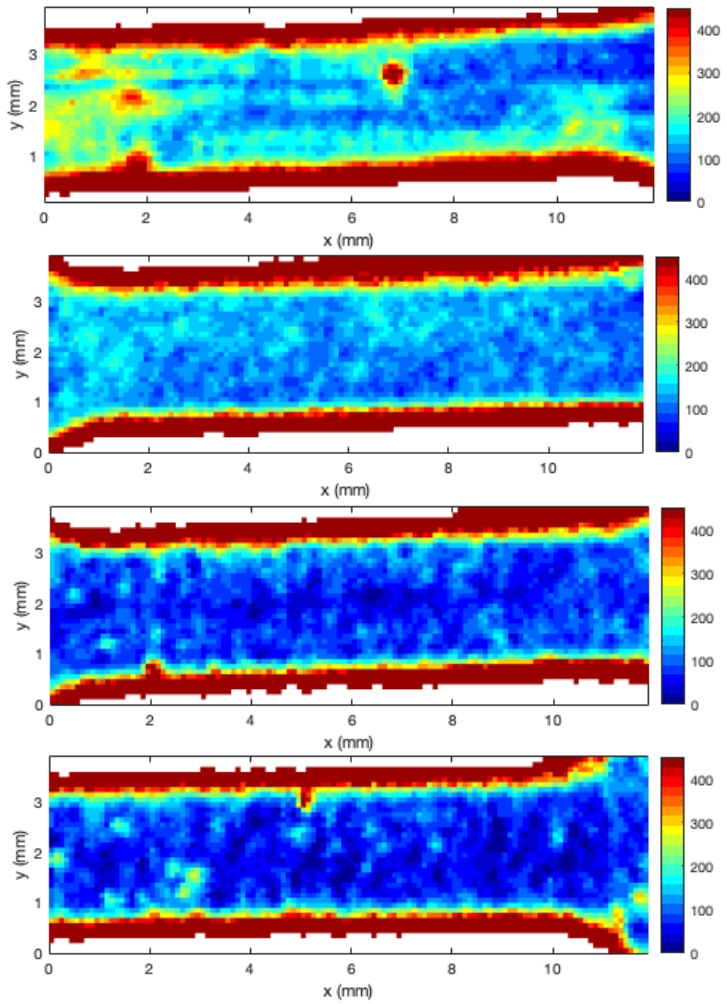

Figure 8: From top to bottom, the martensite, austenite, AM FT and AM ST sample attenuation maps. X and Y values are in mm and show the dimensions of the scan. The color bar is in units of Np/m showing how the energy from the initial pulse decreases throughout the sample. The high attenuations at the edges are due to edge effects and are not analyzed.

Figure 8 shows the attenuation maps of the four NiTi samples. It is immediately evident that the wrought martensite sample has two points of high attenuation in the middle of the sample. Attenuation occurs when the signal is either scattered or absorbed. Therefore, these discontinuities could be from a high concentration of precipitates or impurities during processing which would cause scattering. Differently oriented grains within the sample could also lead to scattering and attenuation. Because martensite has both grain boundaries and a lamella-like structure within the boundaries, it is more susceptible to high attenuation than austenite which only has boundaries between grains. Of these boundaries, both coherent and incoherent boundaries can cause attenuation, though in different ways due to absorption and scattering. Any of these reasons could be why there are two localized areas of high attenuation within the martensitic structure, though more testing is needed to know for sure. It is also noteworthy that the martensite sample has a streak of attenuation in the middle-left side of the sample between 0 and 2 mm in the x-direction and 1 and 3 mm in the y-direction. This is likely because when the samples were machined from a larger block of NiTi, this specific sample was taken partially from the outside of the larger block and partially from the inside. The different grain structure at the edge of the block caused the martensite sample to attenuate differently in that region. The austenite sample shows a more homogenous map, and therefore was likely only cut from one section of the bar. The remaining samples have a more homogenous attenuation map, as evidenced by the smaller error bars shown in Figure 9. Heterogeneity in the martensite sample provides further evidence that the presence of more grain boundaries leads to inconsistent scattering of the ultrasonic signal, shown by a larger error bar. The austenite sample also boasts a higher average attenuation than the AM samples, though not as high as the martensite sample. The higher attenuation in the wrought samples could be due to their anisotropy causing more

scattering, but further testing needs to be done to confirm such a hypothesis. The anisotropic nature of the wrought samples is something of great impact throughout testing. Due to the hot or cold working used to produce wrought samples, the samples become textured meaning they have a preferential grain orientation in the loading direction. This grain orientation affects how the ultrasonic waves propagate through the material which then affects the ultrasonic attenuation and wave speed maps. The AM samples are formed layer by layer, and therefore have no preferential grain orientation and it can be reasonably assumed that the AM samples exhibit bulk-scale isotropic properties relative to the anisotropic wrought samples. This dichotomy is elaborated upon in the results below.

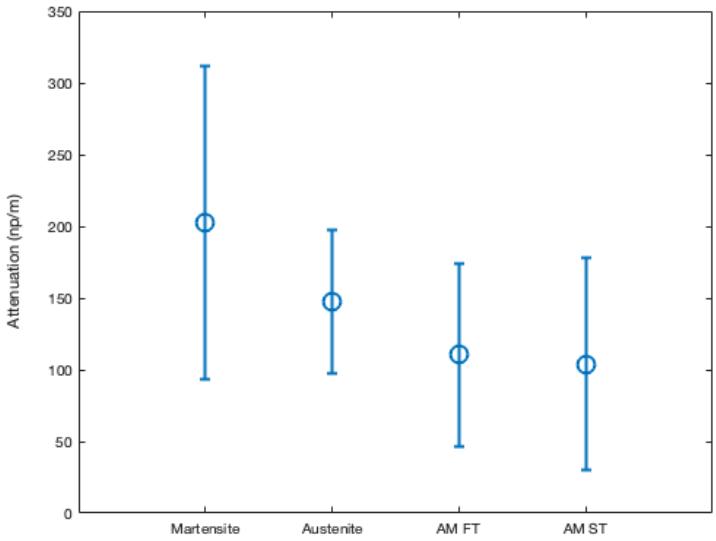

Figure 9: Average attenuation values of the four samples with error bars. The wrought martensite sample had the highest average attenuation, bolstered by the two discontinuities of large attenuation and what is assumed to be a different grain structure machined from the edge of the initial block. Because of these areas of unusually high attenuation, the standard deviation for the martensite sample is also the largest. The AM samples both have a smaller average attenuation than either of the wrought samples, with similar standard deviations.

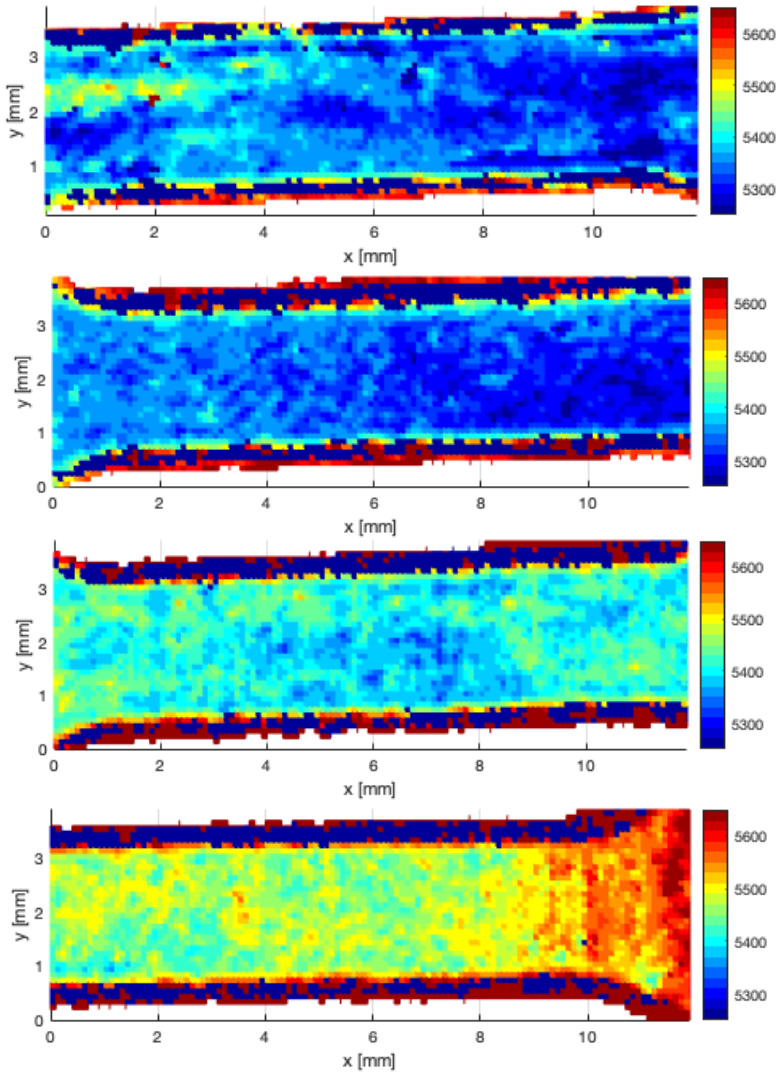

Figure 10: From top to bottom, the martensite, austenite, AM FT and AM ST sample wave speed maps. X and Y values are in mm and show the dimensions of the scan. The color bar is in units of m/s showing the wave speed of the pulse through the sample. Like attenuation, the high speeds at the edges are due to edge effects and are not analyzed.

Figure 10 shows the wave speeds through the four samples. As in the attenuation maps, the martensite sample has a sliver of discontinuity between 0 and 2 mm in the x-direction and 1 and 3 mm in the y-direction due to what is assumed to be different grain structures at different points in the initial block of NiTi that the martensite sample was machined from. Aside from this sliver, all four samples are more or less homogenous throughout. In the martensite sample, the spots of high attenuation that can be seen in Figure 8 do not appear in the wave speed measurements. This shows that the discontinuities present in the sample do not significantly

change the effective properties of the sample in the direction of wave propagation. Unlike with attenuation, the wave speed measurements were considerably higher for the AM materials rather than the wrought materials. This can be seen in both Figures 10 and 11. The error bars for all four samples were relatively large in the wave speed measurements, which is something to focus on, investigate, and hopefully alleviate in future experiments. As noted previously, the anisotropic nature of the wrought samples could lead to lower wave speed within them. Testing the same samples at a different orientation with respect to the transducer could yield different results than the ones presented here because they will interact with the grains in different ways depending on whether or not the grains have a preferential orientation.

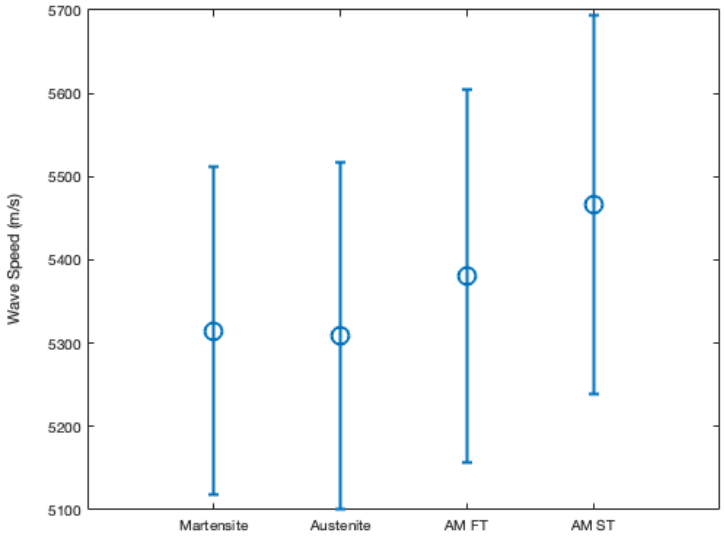

Figure 11: Average wave speed values of the four samples with error bars. Both AM samples had considerably larger wave speed means than either of the wrought samples. Relatively high anisotropy could be the reason for such low values in the wrought samples. All four samples have large error bars which is desirable to cut down on.

Figure 12 was provided by the Hamilton group and shows the stress/strain curves of the five samples tested. The tensile tests used to formulate the plots measured engineering strain by measuring the cross-head displacement. Therefore, instead of showing purely quantitative values, the plot shows relative curves which are still beneficial for analyzing the relationship between elastic moduli and wave speed. Looking at the four NiTi samples, it is clear that the austenite

sample has the highest modulus of elasticity, followed by the AM ST, martensite, and AM FT samples. Due to the high anisotropy of the wrought samples, the AM and wrought samples must be isolated from each other in order to interpolate accurate hypotheses with respect to the wave speed values and the moduli of elasticity. For all samples, the tensile tests used to obtain the stress/strain curves were sensitive to a different direction than the ultrasonic measurements taken. This manifests itself largely in the wrought samples, because the anisotropy of the wrought samples leads to different properties in the through-thickness direction that the ultrasonic measurements were taken in and the perpendicular direction that the tensile tests were done in. Therefore, it is hard to correlate information about the moduli of elasticity of the wrought samples to the wave speed measurements. For example, though it is usually the case that a higher Young's Modulus leads to higher wave speed in the sample, in these results austenite has a lower average wave speed despite having a significantly higher Young's Modulus than the martensite sample. Figure 12 is more beneficial in deducing information about the AM samples.

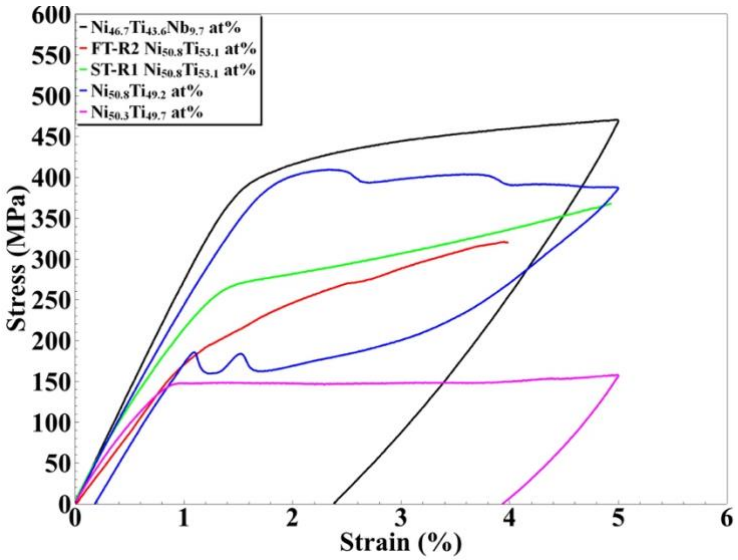

Figure 12: Stress/Strain Curves of the five samples tested provided by the Hamilton group.

The AM ST sample has a higher Young's Modulus than the AM FT sample which corresponds to a higher average wave speed for the AM ST sample. This relationship is expected

because wave speed and modulus of elasticity are directly proportional. The fact that the results match up with the expectation further back the assumption that the AM samples are relatively isotropic.

The anisotropy of the wrought samples was likely the culprit of most of the discrepancies found in testing. Because uniaxial tensile testing and ultrasound are sensitive to different factors specified by grain orientation, conflicting results were gathered. While the relatively isotropic AM samples showed consistent results, with a high average wave speed correlating to a high Young's Modulus, the anisotropic wrought samples paired a lower average wave speed with a higher modulus of elasticity. It is reasonable to conclude that microscale factors manifesting themselves in the wrought samples likely contribute to opposite trends in ultrasonic and mechanical testing. In the future, it is advisable to test more wrought samples with ultrasound in more orientations to correct these opposing trends. More testing is especially beneficial for the wrought samples which not only have different compositions from each other, but are also in different microstructural phases. It is also advisable to do further testing at different temperatures to isolate martensitic and austenitic samples, as well as doing mechanical and ultrasonic testing in the same direction.

SUMMARY, CONCLUSIONS, AND FUTURE WORK

Summary

A large study of SMA microstructures should be completed in order to make them cheaper and to better understand their potential applications. Here, a preliminary study was done on five SMAs in the hopes of attributing certain ultrasonic phenomena with specific mechanical and microstructural causes, to lay out a procedural guideline going forward. The NiTiNb cast sample had to be separated due to its presence of Nb, but was still beneficial in highlighting ultrasound's capability of mapping out eutectic structures and grain boundaries. The AM samples had lower attenuation than the wrought samples, but much higher wave speeds which is likely attributed to the relative isotropy of the AM samples allowed for by their manufacturing. The anisotropy of the wrought samples created conflicting results between the mechanical testing provided by the Hamilton group and the ultrasonic testing. For example, while the AM samples had higher wave speeds corresponding to higher moduli of elasticity, the wrought samples showed opposing trends. In future testing, ultrasonic tests should be conducted in different orientations with respect to the wrought samples including the direction that uniaxial tensile testing is sensitive to.

Conclusions

Testing provided several observations about the relationship between ultrasound, microstructures and isotropy:

- Ultrasound is comparable to SEM imaging in displaying eutectic structures, but is more sensitive to the length-scale resolution of grain boundaries.

- The lamella-like structure within the wrought martensite likely led to a higher attenuation than the other samples through scattering and/or absorption.
- The two isolated areas within the martensitic wrought sample did not significantly affect wave propagation and therefore do not manifest themselves in the wave speed measurements.
- The high anisotropy of the wrought samples led to conflicting trends between moduli of elasticity and wave speed measurements implying that ultrasound and mechanical testing are sensitive to different phenomena and orientations with respect to grains.
- The AM samples were relatively isotropic and provided consistent results, further backing the hypothesis explained above.

Future Work

As discussed throughout the previous sections, the results shown are part of a preliminary study that has the potential to lead to a much larger study that would investigate many more samples differentiated by manufacturing process and tested throughout different points of deformation. As highlighted frequently, the high anisotropy of the wrought samples made it difficult to correlate ultrasonic measurements with microstructural phenomena. Many more tests will be required in order to more accurately understand the microstructures of NiTi SMAs manufactured differently. Hopefully, the results and processes shown above will help make such a study more efficient and consistent. Because SMAs are used so frequently across the world, doing such a broad study in the future could have impacts globally. Through making SMAs cheaper and more prevalent, they can help lead the way to environmental and societal change. Using ultrasound to characterize their microstructures is an excellent start.

REFERENCES CITED

1. Rao. *Introduction to Shape Memory Alloys*, 2015, file:///Users/Trevor/Downloads/Rao2015_Chapter_IntroductionToShapeMemoryAlloy.pdf.
2. Bird, Kevin, et al. "Shape Memory Alloys." *NanoInfo Smart Materials*, Standford University, web.stanford.edu/group/mota/education/Physics%2087N%20Final%20Projects/Group%20Delta/sam.html.
3. *Exploring Shape Memory Alloys*. Georgia Institute of Technology , 2007, www.nnin.org/sites/default/files/files/NNIN-1030_0.pdf.
4. "Everything You Need to Know About Nitinol Wire." *Carl Stahl Sava Industries*, 13 Nov. 2019, www.savacable.com/everything-you-need-to-know-about-nitinol-wire.
5. Kapoor, Deepak. "Nitinol Parts for Stents: Nickel Titanium Shape Memory Alloys." *Johnson Matthey Technology Review*, Johnson Matthey Inc, 2017, www.technology.matthey.com/article/61/1/66-76/.
6. Swardz, Savannah. "How Shape Memory Alloys Work." *Shape Memory Alloys*, University of Washington, depts.washington.edu/matseed/mse_resources/Webpage/Memory%20metals/how_shape_memory_alloys_work.htm#:~:text=Shape%20memory%20alloys%20display%20two%20distinct%20crystal%20structures%20or%20phases.&text=When%20the%20alloy%20is%20heated,had%20before%20it%20was%20deformed.
7. "Transmission Electron Microscope (TEM) - Uses, Advantages and Disadvantages." *MicroscopeMaster*, www.microscopemaster.com/transmission-electron-microscope.html.
8. Filleter T., Beese A.M. (2016) In Situ Transmission Electron Microscopy: Mechanical Testing. In: Bhushan B. (eds) Encyclopedia of Nanotechnology. Springer, Dordrecht. https://doi.org/10.1007/978-94-017-9780-1_100990
9. Liao, Yougui. "History of TEM." *Practical Electron Microscopy and Database*, GlobalSino, 2006, www.globalsino.com/EM/page4539.html.
10. Hans-Joachim Kleebe, Wolfgang Braue, Hans Schmidt, Giuseppe Pezzotti, Günter Ziegler,Transmission electron microscopy of microstructures in ceramic materials,Journal of the European Ceramic Society,Volume 16, Issue 3,1996, https://www.sciencedirect.com/science/article/pii/0955221995001743
11. Xi-Feng Li, Wei Ding, Jian Cao, Li-Yan Ye, Jun Chen. In Situ TEM Observation on Martensitic Transformation during Tensile Deformation of SUS304 Metastable Austenitic Stainless Steel. *Acta Metallurgica Sinica(English Letters)*, 28(3): 302-306
12. "Digital Image Correlation." *Digital Image Correlation - an Overview | ScienceDirect Topics*, www.sciencedirect.com/topics/engineering/digital-image-correlation.
13. "Digital Image Correlation (DIC): 3D Full-Field Measurement." *Dantec Dynamics | Precision Measurement Systems & Sensors*, Dantec Dynamics, 2 Sept. 2020, www.dantecdynamics.com/solutions-applications/solutions/stress-strain-espi-dic/digital-image-correlation-dic/.
14. Bourgeois, Nadine, et al. "Measurement of Local Strain Heterogeneities in Superelastic Shape Memory Alloys by Digital Image Correlation." *Physics Procedia*, Elsevier, 7 Jan. 2011, www.sciencedirect.com/science/article/pii/S1875389210007650.
15. Guisbiers, Gregory, et al. "The Physics of Macro-, Micro-, and Nanomaterials." *Physicalia Magazine*, 2005, file:///Users/Trevor/Downloads/26-PhysicMagazine2005_Thephysicsmacromicronano.pdf.
16. "What Is Non-Destructive Testing (NDT)? Methods and Definition." *TWI*, TWI, www.twi-global.com/technical-knowledge/faqs/what-is-non-destructive-testing.

17. Rhodes, Dr. Kent, and Mary Stellmack. “Back to Basics: Nondestructive Materials Testing.” *Quality Magazine RSS*, Quality Magazine, 14 Sept. 2012, www.qualitymag.com/articles/90473-back-to-basics-nondestructive-materials-testing.
18. P. Šittner, V. Novák, M. Landa, P. Lukáš, Deformation processes in functional materials studied by in situ neutron diffraction and ultrasonic techniques,Materials Science and Engineering: A, Volume 462, Issues 1–2, 2007, Pages 12-22, https://www.sciencedirect.com/science/article/pii/S0921509306019162
19. Stoklasová, Pavla, et al. "In-situ laser-ultrasonic characterization of austenite-martensite transformation." http://congress.cimne.com/smart2017/admin/files/fileabstract/a125.pdf
20. Hu, Eryi, and Wenjin Wang. “The Elastic Constants Measurement of Metal Alloy by Using Ultrasonic Nondestructive Method at Different Temperature.” *Mathematical Problems in Engineering*, Hindawi, 6 Jan. 2016, www.hindawi.com/journals/mpe/2016/6762076/.
21. Papadakis, E. P., et al. “An Ultrasonic Technique for Measuring the Elastic Constants of Small Samples.” *SAE Transactions*, vol. 104, 1995, pp. 830–837. *JSTOR*, www.jstor.org/stable/44473294. Accessed 8 Mar. 2021.
22. “LUMet® : Laser Ultrasonic Sensor for In-Situ Metallurgical Microstructure Studies.” *Laser Ultrasonic Measurement System (LUMet)*, Gleeble, www.gleeble.com/products/specialty-systems/laser-ultrasonic-measurement-system-lumet.html.
23. Sedlak, Petr, et al. “Softening of Shear Elastic Coefficients in Shape Memory Alloys Near the Martensitic Transition: A Study by Laser-Based Resonant Ultrasound Spectroscopy.” *Metals*, vol. 10, no. 1383, 16 Oct. 2020.
24. Deng, Cheri X, et al. “Ultrasound Imaging Techniques for Spatiotemporal Characterization of Composition, Microstructure, and Mechanical Properties in Tissue Engineering.” *Tissue Engineering. Part B, Reviews*, Mary Ann Liebert, Inc., Aug. 2016, www.ncbi.nlm.nih.gov/pmc/articles/PMC4964754/.
25. “Five Industries Utilizing 3D Printing.” *Markforged*, 2020, markforged.com/resources/blog/five-industries-utilizing-3d-printing.
26. W.P.. Mason, H.J.. McSkimin, et al. “Characterization of Grain Size and Yield Strength in AISI 301 Stainless Steel Using Ultrasonic Attenuation Measurements.” *Journal of Nondestructive Evaluation*, Springer-Verlag, 1 Jan. 1974, link.springer.com/article/10.1007/s10921-012-0134-z.
27. Sotelo, Luz D., et al. “Ultrasonic Mapping of Hybrid Additively Manufactured 420 Stainless Steel.” *Ultrasonics*, Elsevier, 7 Oct. 2020, www.sciencedirect.com/science/article/pii/S0041624X20302079.
28. Sealy, M.P., et al. “Glocal Integrity in 420 Stainless Steel by Asynchronous Laser Processing.” *CIRP Annals*, Elsevier, 4 May 2019, www.sciencedirect.com/science/article/pii/S0007850619301374.

29. Arhamnamazi, Seyyedabbas & Bani, Nasrollah & Bani Mostafa Arab, Nasrollah & Refahi Oskouei, Amir & Aymerich, Francesco. (2019). Accuracy Assessment of Ultrasonic C-scan and X-ray Radiography Methods for Impact Damage Detection in Glass Fiber Reinforced Polyester Composites. Journal of Applied and Computational Mechanics. 5. 10.22055/JACM.2018.26297.1318.

30. *Immersion Transducers*, www.olympus-ims.com/en/ultrasonic-transducers/immersion/.
31. Hamilton, R.F., Lanba, A., Ozbulut, O.E. *et al.* Shape Memory Effect in Cast Versus Deformation-Processed NiTiNb Alloys. *Shap. Mem. Superelasticity* **1,** 117–123 (2015). https://doi.org/10.1007/s40830-015-0024-1

APPENDIX A

```
% Wavespeed Code- modified by Olivia Jan 2021 for 3M project samples
clc, clear,close all
% Opens and loads in the data file you want to analyze
[fileName,pathname] = uigetfile('*.*','Choose file to open');
%% Variables-- Make sure to change these when switching samples
t = 1.016e-3; % sample thickness in m
thickness_silica = 1.5875;
wp_diff = -3.114e-3;%Wp for silica - Wp for sample converted from mm to m

c_water = 1486;
rho_water = 1000;
rho_sample = 6500;
rho_silica = 2200;
%% Reading information from file- I suspect this needs tweaked for new
versions of MATLAB
fid = fopen([pathname, fileName],'r'); % File name
B = textscan(fid,'%s','Delimiter','\tab','HeaderLines',8); %ignoring first 8
lines of data files
s = strrep(cell2mat(B{1}(2)),' ','a'); s2 = s(~isspace(s)); s2 =
regexp(s2,'\d?\.?\d+','match');
ad_delay = str2double([s2{1} s2{2}]); % in microseconds
s = strrep(cell2mat(B{1}(3)),' ','a'); s2 = s(~isspace(s)); s2 =
regexp(s2,'\d?\.?\d+','match');
% ad_width = str2double(s2); %[s2{1} s2{2}]); % in microseconds
ad_width = str2double(s2); % [s2{1} s2{2}]); %in microseconds
s = strrep(cell2mat(B{1}(8)),' ','a'); s2 = s(~isspace(s)); s2 =
regexp(s2,'\d?\.?\d+','match');
ad_rate = str2double([s2{1} s2{2}]); % in MHz
Fs = ad_rate*1e6; %sampling frequency in Hz
time_vec = ad_delay:1/ad_rate:(ad_delay+ad_width-1/ad_rate);

fid = fopen([pathname,fileName],'r'); % File name
D = textscan(fid,'%s','Delimiter','\tab','HeaderLines',36); %ignoring first
49 lines of data files
s = strrep(cell2mat(D{1}(2)),' ','a'); s2 = s(~isspace(s)); s2 =
regexp(s2,'\d?\.?\d+','match');
%x_w = str2double(s2);%[s2{1} s2{2}]); % scanning axis length
x_w = str2double([s2{1} s2{2}]); %s2);% scanning axis length
s = strrep(cell2mat(D{1}(4)),' ','a'); s2 = s(~isspace(s)); s2 =
regexp(s2,'\d?\.?\d+','match');
x_res = str2double(s2); % scanning axis resolution
s = strrep(cell2mat(D{1}(6)),' ','a'); s2 = s(~isspace(s)); s2 =
regexp(s2,'\d?\.?\d+','match');
y_w = str2double(s2); % index axis length
s = strrep(cell2mat(D{1}(7)),' ','a'); s2 = s(~isspace(s)); s2 =
regexp(s2,'\d?\.?\d+','match');
y_res = str2double(s2);     % index axis resolution
NN = round(x_w/x_res/2 * y_w/y_res/2 - x_w/x_res/2); % selects reference
waveform from middle of sample
x_vec= 0:x_res:(x_w-x_res);
y_vec= 0:y_res:(y_w-y_res);
%% Read Data Files
fid = fopen([pathname, fileName],'r'); % File name of Sample
C = textscan(fid,'%s','Delimiter','\tab','HeaderLines',49);
```

```
%ignoring first 49 lines of data files
for i = 1:length(C{1})-1
    s = cell2mat(C{1}(i)); s = strrep(s,' ','a'); s2 = s(~isspace(s));  s3 =
strrep(s2,'aaa',' ');
    wf_t = str2num(s3);
    wf_t = wf_t(3:end);
    if i == 1
        wf_data = zeros(length(C{1})-1,length(wf_t));
        size(wf_data);
    end
    wf_data(i,:) = wf_t;    % matrix with all waveforms, each row is a
scanning position
end
%% Select Front Wall and 3 Back Walls for FFTs %%
% used for the program to identify the sections of signal you are going
% to analyze (ignores some of the noise)
figure(3), plot(wf_data(NN,:))
% plots the amplitude of signal somewhere in middle of sample
ylabel('Amplitude')
hold on
answer1= questdlg('Select two points that encompass the front wall',
'waveform selection', 'OK', 'I can''t','cancel','cancel');
while strcmp(answer1, 'I can''t')==1
    cla
    NN=NN+20;
    plot(wf_data(NN,:))
    answer1= questdlg('Select two points that encompass the front wall',
'waveform selection', 'OK', 'I can''t','cancel','cancel');
end
if strcmp(answer1, 'cancel')==1
    error('Please select "OK" or select "I can''t" in order to choose a
different reference waveform')
end
Cut_1 = round(ginput(2));
wf_fw = wf_data(:,Cut_1(1,1):Cut_1(2,1));
questdlg('Select two points that encompass the first back wall');
Cut_2 = round(ginput(2));
wf_bw= wf_data(:,Cut_2(1,1):Cut_2(2,1));
hold off
%% Creating separate vectors of backwall waveforms
% To find the time delay here we want to take the cross correlation (xcorr)
% of 2 different back walls.  We want to pad all the other values with
% zero.
fw = zeros(size(wf_data));
fw(:, Cut_1(1,1):Cut_1(2,1))= wf_fw;
bw = zeros(size(wf_data));
bw(:, Cut_2(1,1):Cut_2(2,1))= wf_bw;
%% Wavespeed calculatiosn using cross-correlation
delay_sample = zeros(1,size(fw,1));
for ii=1:size(fw,1)
    [corr,lags]= xcorr(fw(ii,:), bw(ii,:));
    [~,delay1]= max(-(corr));
    delay_sample(ii) = -lags(delay1);
end
time_delay= delay_sample./Fs;
wavespeed= 2*t./time_delay;
wavespeed(max(bw,[],2)<0.02) = NaN;
```

```
%%
% Now we have the unfiltered wavespeed vector. We need to get rid of the
% places where there is no signal and also get rid of the outliers
wavespeed_avg = mean(wavespeed,'omitnan' )
wavespeed_std = std(wavespeed, 'omitnan')
wavespeed_mat= zeros(length(y_vec),length(x_vec));
for i=1:(length(y_vec))
    wavespeed_mat((end-(i-1)),:)= wavespeed((1:length(x_vec))+(i-
1)*length(x_vec));
end
num_bins= 20;
surf(x_vec,y_vec,wavespeed_mat,'EdgeColor','flat'),caxis([min(rmoutliers(wave
speed)) max(rmoutliers(wavespeed))])
view([0 90]), axis equal, axis tight
colormap(jet(num_bins)); colorbar
xlabel('x [mm]')
ylabel('y [mm]')
caxis([5250,5650])

questdlg('Please select the Top right corner and then the bottom left corner
of the inside area');
inside_edges= round(ginput(2));
inside_r= inside_edges(1,2):inside_edges(2,2);
inside_c= inside_edges(1,1):inside_edges(2,1);
wavespeed_avg_inside= mean(wavespeed_mat(inside_r-y_vec(1), inside_c-
x_vec(1)), 'all', 'omitnan');
wavespeed_outside= wavespeed_mat;
wavespeed_outside(inside_r, inside_c)= NaN;
wavespeed_avg_outside= mean(wavespeed_outside, 'all', 'omitnan');
%%
N = 2^(nextpow2(size(bw,2))+3); % number of points for FFT, ensure it's
greater than length of wf_bw1/2/3
f_c = (0:N/2-1)*ad_rate/N; % frequency vector based on sampling rate
% First back wall
F_bw1 = fft(bw',N);
F_bw1 = abs(F_bw1(1:N/2,:));

%%
[fileName,pathname] = uigetfile('*.*','Open silica file');
fid = fopen([pathname fileName],'r'); % File name
C = textscan(fid,'%s','Delimiter','\tab','HeaderLines',49);
for i = 1:length(C{1})-1
    s = cell2mat(C{1}(i)); s = strrep(s,' ','a'); s2 = s(~isspace(s)); s3 =
strrep(s2,'a',' ');
    wf_t = str2num(s3);
    if i == 1
        wf_data_silica = zeros(length(C{1})-1,length(wf_t));
    end
    wf_data_silica(i,:) = wf_t;
end
wf_data = wf_data_silica(:,2);

%%
% figure(10),plot(wf_data)
bw_silica1 = zeros(size(wf_data));
bw_silica2 = zeros(size(wf_data));
```

```
% questdlg('Select two points that encompass the first back wall');
% Cut_1 = round(ginput(2));
Cut_1 = [1163,0;1389,0];
bw_silica1(Cut_1(1,1):Cut_1(2,1)) = wf_data(Cut_1(1,1):Cut_1(2,1));
% questdlg('Select two points that encompass the second back wall');
% Cut_2 = round(ginput(2));
Cut_2 = [1712,0;1889,0];
bw_silica2(Cut_2(1,1):Cut_2(2,1)) = wf_data(Cut_2(1,1):Cut_2(2,1));
%%
[corr,lags]= xcorr(bw_silica1, bw_silica2);
[~,delay1]= max(corr);
delay_silica = -lags(delay1);
c_silica = 2*thickness_silica./(delay_silica/ad_rate)*1e3;
%%
F_bw_silica = fft(bw_silica1,N);
F_bw_silica = abs(F_bw_silica(1:N/2,:));
%% attenuation
alpha_water = 25.3e-15*(f_c*1e6).^2;
c_sample = wavespeed;
R_sample = (c_sample*rho_sample-
c_water*rho_water)./(c_sample*rho_sample+c_water*rho_water);
R_silica = (c_silica*rho_silica-
c_water*rho_water)/(c_silica*rho_silica+c_water*rho_water);
att = 1./(2*t).*log((F_bw_silica./F_bw1).*(R_sample.*(1-
R_sample.^2))./(R_silica*(1-R_silica^2)).*exp(2*alpha_water.*wp_diff)');
att(:,max(bw,[],2)<0.02) = NaN;
%%
center_freq_ind = find(f_c > 20 & f_c < 22,1,'first');
att_cf = att(center_freq_ind,:);
att_mat= zeros(length(y_vec),length(x_vec));
for i=1:(length(y_vec))
   att_mat((end-(i-1)),:)= att_cf((1:length(x_vec))+(i-1)*length(x_vec));
end
h2 = figure(2);
surf(x_vec,y_vec,att_mat),view([0 90]),caxis([0 max(rmoutliers(att_cf))])
xlabel('x (mm)')
ylabel('y (mm)')
shading flat, axis equal, axis tight, colormap(jet(num_bins)), colorbar, grid
off, box on
caxis([0,450])
cent_freq = f_c(center_freq_ind)
att_mean = mean(rmoutliers(att_cf),'omitnan')
att_std = std(rmoutliers(att_cf),'omitnan')
att_avg_inside= mean(att_mat(inside_r-y_vec(1), inside_c-x_vec(1)), 'all',
'omitnan');
att_outside= att_mat;
att_outside(inside_r, inside_c)= NaN;
att_avg_outside= mean(att_outside, 'all', 'omitnan');
```

ACADEMIC VITA

Trevor Grim

EDUCATION

The Pennsylvania State University **Class of 2021**
Schreyer Honors College, *College of Engineering* *University Park, PA*
Bachelor of Science (B.S.) in Engineering Science and Mechanics
Skilled in NX, Solidworks, NX, C++ and MATLAB

WORK AND VOLUNTEER EXPERIENCE

Northrop Grumman **May 2019 – August 2020**
Mechanical Engineering Intern-Mechanical Technology Group *Linthicum, MD*
- Worked with subject matter experts daily to design new testing apparatuses
- Obtained Department of Defense Secret Level Security Clearance
- Design lead of an 8-person team on a real-world project lasting 10 weeks with a $2000 budget
- Designed and built full scale model of belly of an F-18
- 3D printed various parts for modeling and testing

Kinsley Construction, Incorporated **May 2018 – August 2018**
Project Estimator *York, PA*
- Work regularly in teams and with subcontractors to compile a price
- Travel to different companies to coordinate bids
- Work through difficult problems to find efficient solutions
- Estimated over $100 million in construction projects

Penn State College of Engineering **August 2019 – Present**
Research Assistant *University Park, PA*
- Perform nondestructive analysis on various materials to find weaknesses
- Develop methods using ultrasound to detect flaws in titanium
- Use MATLAB to analyze data and compile into a publishable research paper

Penn State South Food District **August 2017 – Present**
Server *University Park, PA*
- Take orders and prepare food at the Redifer City Grill during hours of high volume
- Multitask between stations to be as efficient as possible

LEADERSHIP EXPERIENCE

Turning Point USA at Penn State **August 2017 – Present**
President and Campus Coordinator *University Park, PA*
- Lead meetings of over 40 members
- Hosted Donald Trump Jr. at an event that sold over 2200 tickets
- Organize and implement weekly information and recruiting sessions
- Plan campus wide activities such as speakers and events
- Invent innovative ways to promote free speech and free markets

Engineering Orientation Network **April 2018 – August 2020**
Mentor *University Park, PA*
- Work in teams to organize orientation day events
- Manage a team of 15 mentees
- Help advise mentees throughout their freshman year

AWARDS & HONORS

Schreyer Honors College Academic Excellence Scholarship *2017 – 2020*
Conewago Enterprises Scholarship *2017 – 2020*
John D. Bare Memorial Scholarship *2017 – 2020*
The President's Freshman Award *2018*